Engineering Geology xxx (xxxx) xxx

Contents lists available at ScienceDirect

Engineering Geology

journal homepage: www.elsevier.com/locate/enggeo

Improved technical guide from physical model tests for TDR landslide monitoring

Chih-Chung Chung [a], Chih-Ping Lin [b,*], Yin Jeh Ngui [b], Wen-Chin Lin [b], Chun-Shen Yang [b]

[a] Dept. of Civil Engineering/Research Center for Hazard Mitigation and Prevention, National Central University, 300 Zhongda, Rd., Zhongli Dist., Taoyuan 320, Taiwan
[b] Dept. of Civil Engineering, National Yang Ming Chiao Tung University, 1001 Ta-Hsueh, Rd., Hsinchu 300, Taiwan

ARTICLE INFO

Keywords:
Time-domain reflectometry
Landslide monitoring
Shear deformation
Direct shear test

ABSTRACT

Time-domain reflectometry (TDR) can help observe the initiation and evolution of localized shear planes in both rock and soil slopes, and has temporal and spatial resolutions suitable for landslide monitoring. An improved and standardized technical guide for TDR cable installation and data interpretation is needed to utilize it better. TDR technique involves sending an electromagnetic pulse into a coaxial cable grouted in a pre-drilled borehole, and capturing the reflected signal from cable deformity, which is triggered by the localized shear deformation in the underground. This study developed a large direct shear box for testing TDR responses in various cable-grout-ground assemblies, in order to reliably model the cable-grout-ground interaction at the localized shear. Different combinations of cable type, grout condition, soil type, and shear bandwidth were tested using the new physical model to re-examine TDR's response to ground deformation in sliding mode. The results revealed some misconceptions in previous studies that used cable-grout assemblies without considering the entire interaction with the ground. The implications of the experimental results are carefully considered and new technical recommendations are provided for cable installation and data interpretation to foster the improved use of TDR. A new data reduction method that involves data filtering, differential waveform, and three-sigma rule is proposed to support the recommended installation setup for robust early detection of a localized shear plane.

1. Introduction

Locating and monitoring the temporal development of localized shear deformations in a slope is crucial for landslide assessment and slope stabilization (Willenberg et al., 2008a, 2008b; Wolter et al., 2020). In practice, slope inclinometers are used almost exclusively for such a purpose (Allasia et al., 2020; Di Maio et al., 2010). To enhance both the temporal and spatial resolution as well as the cost efficiency for slope monitoring, new technologies are emerging that could either supplement inclinometer logging or partially replace inclinometers in landslide monitoring programs (Sun et al., 2014). There is also a trend to integrate multiple or even redundant observations from different types of sensors for cross examination of landslide displacement and other early warning indicators (Intrieri et al., 2012; Simeoni et al., 2020).

Time-domain reflectometry (TDR) technology, in particular, has become a valuable and convenient tool for continuous monitoring of the development of localized shear deformation in rock (Dowding et al., 1988, 1989; Dowding and Huang, 1994; Pasuto et al., 2000; Su et al., 2009; Thuro et al., 2010) or soil masses (Dowding and Pierce, 1994; O'Connor et al., 1995; Dowding et al., 2001). Nevertheless, the use of TDR in landslide monitoring is relatively uncommon, which may be attributable to the absence of standard guidelines. A comprehensive standard that addresses various factors in TDR cable installation and data interpretation is needed to facilitate the practicability and effectiveness of TDR applications.

TDR is a measurement technique that was first introduced in the 1930s for locating damages in transmission line cables, based on guided electromagnetic (EM) waves. A pulse generator sends an electrical pulse along the cable-under-test, while a waveform sampler is used to observe the returning echoes due to impedance mismatches in the cable. TDR was later better known for measuring dielectric properties by adding a sensing waveguide at the end of the transmission line (Topp and Ferre, 2000; Lin et al., 2015). Revisiting its original function, damage monitoring of a coaxial cable embedded in a slope prone to sliding deformation would turn TDR into a valuable tool for slope stability monitoring. Barendse and Machan (2009) indicated that slope inclinometers can provide the magnitude and the direction of ground deformation, while TDR is primarily employed to locate active shearing

* Corresponding author.
E-mail addresses: cchung@ncu.edu.tw (C.-C. Chung), cplin@mail.nctu.edu.tw (C.-P. Lin), billgates999.cv95g@nctu.edu.tw (C.-S. Yang).

https://doi.org/10.1016/j.enggeo.2021.106417
Received 6 November 2020; Received in revised form 29 September 2021; Accepted 19 October 2021
Available online 6 November 2021

planes. Nevertheless, the amplitude of TDR reflected pulse due to the cable's pinched deformation, is proportional to the sliding displacement of a slope, in which the amplitude can be utilized to estimate the localized shear deformation. Dowding et al. (1988, 1989) and Aimone-Martin et al. (1994) introduced calibration tests to quantify the empirical relationship between the shear displacement in the rock mass and the intensity of the TDR reflection spike. In general, there are several critical influencing factors towards the relationship between TDR reflection signal and shear displacement, including but not limited to cable resistance, cable-grout-ground interaction, and shear bandwidth.

Electrical resistance increases with cable length and results in increased rise time and decreased amplitude on the reflected pulse of the TDR signal. To account for the effect of cable resistance on the amplitude of reflection spike, Kim (1989) and Pierce et al. (1994) introduced an influence chart to demonstrate the effect of different leading cable lengths on a particular cable type and deformation mechanism. Dowding et al. (2002) proposed a finite-difference wave propagation model to simulate the effect of cable resistance and multiple reflections. Lin and Tang (2006) later provided a more comprehensive and efficient wave propagation model that accurately simulates the TDR response including the resistance effect. Based on this model, Lin et al. (2009) suggested a more general correction procedure to compensate for the effect of cable resistance. Therefore, this factor is now satisfactorily addressed in the relationship between the shear displacement and the amplitude of the TDR reflection spike.

The complex cable-grout-ground interaction can further complicate the relationship between TDR reflection amplitude and shear displacement. The compliant cable-grout composite was recommended for site installation to enhance cable deformity in soil slopes (Pierce, 1998; Cole, 1999; Dowding et al., 2001; Dowding et al., 2002; Blackburn and Dowding, 2004). Lin et al. (2009) later conducted tests on cable-grout-ground composites in a long direct shear box (70 mm × 70 mm in cross-section and 400 mm in length) to investigate the effect of cable-grout-ground interaction as well as shear bandwidth. They found out that the compliance problem (e.g., grout stiffer than surrounding soil) is not critical. Instead, a tensile crack of the stiff (but low tensile strength) armored grout would develop near the sliding plane, where the fractured grout would then facilitate cable deformity in response to the shear displacement. Festl (2008) and Singer (2010) conducted extensive laboratory shear tests with different cable-grout assemblies to investigate the amount of displacement required to generate a detectable TDR signal. They focused on the cable-grout assembly (instead of cable-grout-ground composite in actual field condition) and showed that the TDR signal amplitude strongly depended on the grout strength and shear zone width (Thuro et al., 2010).

The effect of shear bandwidth further complicates the relationship between the shear displacement and TDR reflection amplitude. O'Connor (1991) and O'Connor et al. (1995) modeled the shear band by including an air gap in the grout during shear tests on cable-grout composites. They observed that TDR signal amplitudes decreases as the gap increases, while double reflections may occur when the air gap is large. However, a rather different behavior was observed by Lin et al. (2009) in their direct shear tests of cable-grout-ground assemblies in a long direct shear box, in which a width of soil layer on the shear plane was replaced by weak clay, to form a realistic shear band without a gap in the grout. Their results showed that larger shear bandwidth would require larger shear displacement to mobilize the detectable TDR reflection. However, once the cable deformation and TDR reflection are mobilized, the relationship between the shear displacement and TDR reflection amplitude would be relatively independent of shear bandwidth.

As seen from the literature review above, previous investigations were mainly conducted on cable-grout assemblies without surrounding materials. Lin et al. (2009) revealed the impact degree of shear bandwidth, cable resistance, and cable-grout-ground interaction to the TDR response from their direct shear tests on cable-grout-ground assemblies in a long direct shear box. However, a much larger shear box without boundary effects in both transverse and longitudinal directions is required to physically model the shear zone in full scale and to investigate the cable-grout-ground interaction more realistically. In light of this, the objective of this study was to develop such a large direct shear test for cable-grout-ground assemblies. Different combinations of cable, grout, ground, and shear bandwidth were tested using the new physical model, in order to re-examine potential influencing factors that would affect the TDR's response to the localized shear deformation. Implications for the optimization of TDR cable installation and data interpretation were subsequently discussed based on physical model tests.

2. TDR basics

A TDR measurement setup comprises of a TDR device and a transmission line system, as shown in Fig. 1. The TDR device generally consists of a pulse generator, a sampler, and an oscilloscope. The transmission line is composed of a leading coaxial cable and a sensing waveguide. The sensing waveguide may be the coaxial cable (e.g., for landslide deformation) itself or a specially-designed multi-conductor waveguide for dielectric measurements. The pulse generator sends an EM step pulse into the lead cable, while the sensing waveguide further directs the EM wave into the material-under-test or the environment to be monitored.

TDR wave propagation is a function of the propagation constant γ and the characteristic impedance Z_c. The former factor controls the velocity and attenuation (Eq. 1), while the latter term affects the magnitude of reflection (Eq. 2) in the following relations for coaxial waveguides (Lin and Tang, 2006):

$$\gamma = \frac{j2\pi}{c}\sqrt{\varepsilon_r^*}\cdot A \tag{1}$$

$$Z_c = \frac{Z_p}{\sqrt{\varepsilon_r^*}}\cdot A \tag{2}$$

$$A = \sqrt{1 + \frac{(1-j)\,\alpha_R}{\sqrt{f}}} \tag{3}$$

where c is the speed of light, $\varepsilon_\gamma{}^*$ the relative dielectric permittivity of the material between conductors, A the resistance effect factor, Z_p the geometric impedance (i.e., characteristic impedance in free space); j the complex unit, f the frequency, and α_R ($\sec^{-0.5}$) the resistance loss factor. The geometric impedance Z_p depends on the size, configuration, and spacing of the waveguide conductors. For a coaxial cable, the impedance decreases as the spacing between inner conductor and outer conductor decreases. According to Eq. (2), the electrical characteristic impedance changes as the sensing waveguide is subjected to deformation that changes its cross-sectional geometry or when the electrical properties of

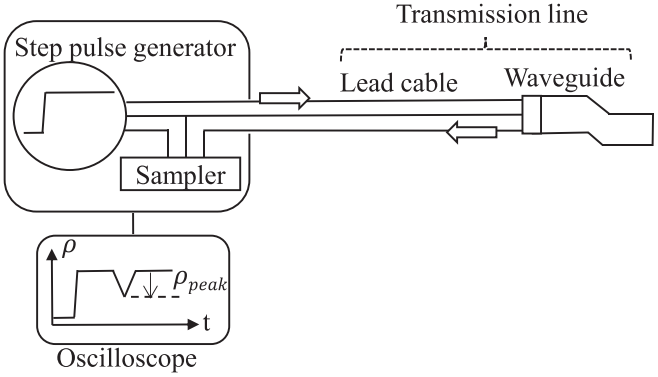

Fig. 1. A typical configuration of TDR system.

the sensing medium (between conductors) varies. Reflections occur at the interfaces of impedance change. The reflection coefficient ρ at the i^{th} mismatch interface can be defined as:

$$\rho = \frac{Z_{c,i+1} - Z_{c,i}}{Z_{c,i+1} + Z_{c,i}} \quad (4)$$

where $Z_{c,i}$ and $Z_{c,i+1}$ are the characteristic impedances for i^{th} section and $(i+1)^{th}$ section of the transmission line, respectively.

TDR reflections due to these impedance changes are recorded to deduce the measured information. Through a specially designed multi-conductor waveguide, TDR can be implemented to measure the dielectric characteristics and related physical properties. For example, Tan et al. (2018) developed a plastic-coated probe to measure water content accurately in highly saline soil, while Chung and Lin (2011) used a three-conductor waveguide in water for suspended sediment concentration measurement.

Grouting a coaxial cable into a borehole is comparable to implanting a sensing nerve into the ground. As the localized shear deformation develops within the slope, the sliding plane would deform or pinch the sensing cable, changing its characteristic impedance. The cable's characteristic impedance is reduced when its cross-section is compressed due to the sliding deformation. A negative step reflection occurs as the impedance goes from high to low at the top of the sliding surface, and shortly a positive step reflection follows when the impedance goes from low to high at the bottom of the sliding surface. Therefore, a spike-like negative reflection is induced due to the shearing mechanism of the localized shear deformation. The travel time where the reflection occurs is determined by the location of the sliding plane, while the amplitude of the reflection spike is related to the amount of sliding displacement, which is expressed in terms of the peak reflection spike, ρ_{peak}, as denoted in Fig. 1. It should be noted that it is conventional to present the TDR voltage waveform $v(t)$ in terms of dimensionless reflection coefficient, which is rescaled as $\rho = (v - v_0)/v_0$, where v_0 is the input step voltage and the numerator represents the reflected signal.

3. Physical model of shear zone detection through TDR measurements

Fig. 2 depicts a conceptual model of TDR landslide monitoring. The coaxial cable is deformed at the depth where it intersects the sliding plane of the monitored slope. The inset in Fig. 2 shows how the sliding deformation of the cable-grout-ground composite can be physically modeled by a large direct shear box. The shear displacement and shear bandwidth are denoted as δ and W, respectively.

In order to realistically model the cable-grout-ground interaction in the direct shear box, the boundary effect should be avoided in both the radial and longitudinal directions of the cable-grout assembly. Installation of a TDR cable is mechanically analogous to soil nailing works. When subjected to shearing, the cable and soil nail are stressed near the sliding (shearing) plane. The ground stress acting on the cable-grout assembly can be further simplified by an idealized elastic analysis (Juran and Schlosser, 1986), as illustrated in Fig. 3(a). The half influence length with significant stress acting on the cable-grout assembly is about 3 L_0, in which L_0 was derived as:

$$L_0 = \left[\frac{(4EI_0)}{(K_s D)}\right]^{\frac{1}{4}} \quad (5)$$

where E, I_0, and D are the Young's modulus, moment of inertia, and diameter of the axial element (i.e., the cable-grout composite), respectively, while K_s is the modulus of subgrade reaction. The axial element diameter D of 0.05 m was used to construct the physical model in this study. The estimated values adopted for the material parameters in Eq. (5) were E = 75,000 kPa for the grout (Blackburn and Dowding, 2004) and K_s = 24,430 kN/m^3 in sandy soils (Reese, 1983). Based on these assumptions, L_0 was estimated to be 0.09 m. The half-length of the direct shear box should therefore be larger than $3L_0$ = 27 cm. This study conservatively used 55 cm for the shear box construction, as illustrated in Fig. 4(a). As for the radial direction, the stress influence range can be taken approximately twice the diameter of the cable-grout composite, as shown in Fig. 3(b). Hence, the internal cross-section of the direct shear box was selected as 25 cm × 25 cm, as shown in Fig. 4(b). The detailed design of overall setup, including the detailed support frame and bracing for the large-scale direct shear box, is shown in Fig. 5. At the shear interface, an assembly of sliding sheets is introduced to force the formation of a shear band ranging from 1 cm to 5 cm, at 1 cm interval. The assembly of sliding sheets is illustrated in Fig. 6, while Fig. 7 shows the top-view photo of a fully assembled large direct-shear-box device, along with hydraulic jacks, transducers, and data acquisition systems.

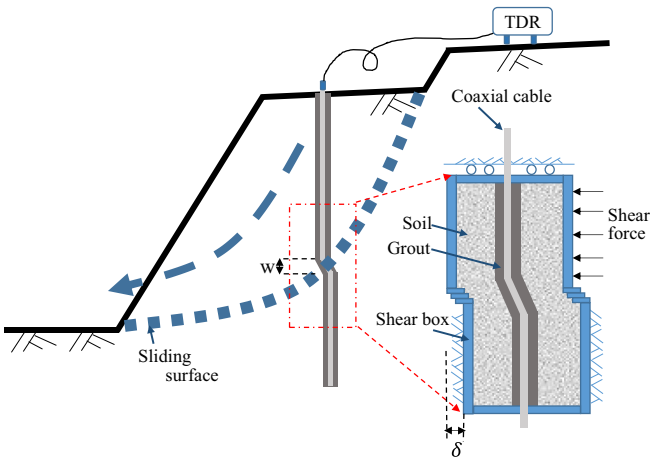

Fig. 2. Physical modeling of TDR shear displacement monitoring (modified from Lin et al., 2009).

Two hydraulic jacks with 10 tons maximum capacity and stroke up to 180 mm were utilized to apply shear force and to provide vertical overburden pressure. A load cell (Futek LCF 450), with 4543 kgf (10,000 lbf) capacity and 0.1% full scale (F.S.) resolution, was installed to monitor the applied overburden pressure. The shear displacement was measured by a LVDT (Gefran LT-M-0200-S) with 200 mm measurement range and 0.01 mm resolution.

Semi-rigid coaxial cables with solid aluminum outer conductors are often used in rocks for high signal quality, while less rigid coaxial cables with braided copper wires as the outer conductors are preferable in soils (Dowding et al., 2002). Fig. 8 shows three types of coaxial cables used in our physical model tests. The CommScope P3-500 JCASS (diameter over jacket = 14.48 mm) and P3-500 CA cables (diameter over outer conductor = 12.7 mm and without jacket) are semi-rigid cables with solid outer conductor shield. In contrast, the Belden RG-8 (diameter over jacket = 10.29 mm) is a flexible coaxial cable with braided wires as the outer shield, which has lower signal attenuation than most other flexible cables (Belden, 2018). Detailed specifications of the cables used are tabulated in Table 1.

The sensing section of the cable was first cast in a 5 cm diameter cylindrical mold using Portland type I cement with 1:1 water/cement ratio, as suggested by Lin et al. (2009). The precast grout column was then placed at the center of the direct shear box that was backfilled with soils. The extended cable length leading to the TDR device was 20 m.

Two types of backfilled materials were used, including Ottawa sand and fine gravel, to represent loose materials and stiffer materials, respectively. The soils were gradually backfilled into the shear box and were moderately compacted. The physical properties of backfilled materials are listed in Table 2. A normal pressure of σ_v = 285 kPa was applied in the axial direction by a confining jack (labeled as 3 in Fig. 7) to simulate an overburden pressure equivalent to 18.5 m of Ottawa sand or 17.5 m of fine gravel. Different combinations of cable type, soil type,

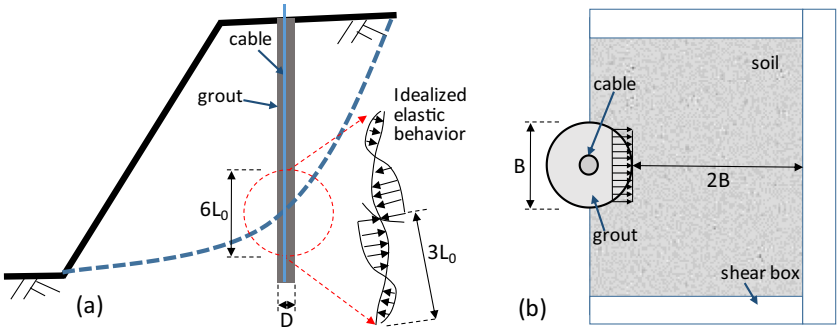

Fig. 3. Considerations of (a) influenced length L_0 in the axial direction (modified after Juran and Schlosser, 1986), and (b) the influence area in the radial direction of the direct shear box.

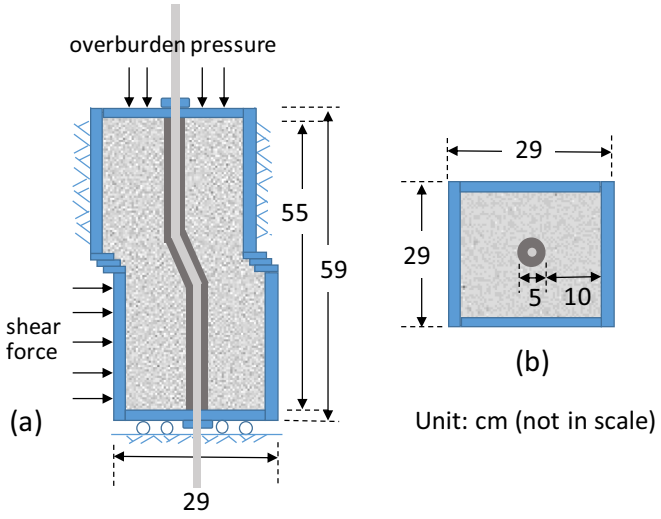

Fig. 4. (a) Top view and (b) side view schematics of the direct shear box.

borehole backfill (native soil vs. grout), and shear bandwidth were tested to re-examine their influences on the TDR response. After the sample was assembled into the direct shear box, the initial waveform was acquired using a TDR device (Tektronics 1502C). The sampling interval was about 14 ps, which corresponds to the division setting of the TDR device of 0.1, while the number of data points in an acquired waveform was 2048. Subsequent TDR waveforms were acquired for every 1 mm of shear displacement on the physical model up to a cumulative displacement of 100 mm.

4. Results and discussion

4.1. Cable-grout-ground composite response of different coaxial cable

Most of the previous performance evaluations on different TDR cables were conducted on cable-grout assemblies instead of the ultimate cable-grout-ground composites in the field. One of the major criterion in cable selection is to have sufficient measurement sensitivity even in weaker grounds. Two major types of coaxial cables that are commonly available were tested, namely the P3-500 and RG-8, representing stiff and soft cables, respectively. In general, a PE jacket is preferred to prevent corrosion on the outer conductor. However, the PE jacket may slip from the smooth surface of the solid aluminum outer conductor in P3-500 cables, thus reducing its sensitivity to shear displacement. Therefore, bare (P3-500) and coated (P3-500 JCASS) cables were tested to evaluate this potential. Fig. 9 shows the measured waveforms of direct shear tests for the three types of cables in loose sands (representing weak grounds) under the prescribed 285 kPa overburden pressure. Dual reflection spikes were observed in Fig. 9, as opposed to the single spike in the results of shearing cable-grout assemblies.

To explain the dual reflection spikes, the deformation and stressed behavior of the cable-grout composite caused by lateral earth pressure is examined. From the embedded photos in Fig. 9, the shearing did not create a sharp cut in the cable-grout composite in weak ground. The cable-grout composite can be considered to behave like a laterally loaded soil nail. The lateral stress, shear force, and bending moments are illustrated in Fig. 10. A distance between points of maximum moments on either side of the shear plane can be derived as $\pi L_0/2$ (Schlosser, 1982). According to Eq. (5), L_0 increases as the modulus of ground decreases. Instead of a single cut, the reverse bending moments near the shear plane induces tension cracks on either side of the shear plane. Further shear displacement enlarges the shear deformation of the coaxial cable along the two tension cracks, resulting in two reflection spikes observed in Fig. 9. The two reflected pulses are more separated in the bare P3-500 cable (Fig. 9(b)) since the stiff cable has more localized kinks, compared to that in the soft braided RG-8 cable (Fig. 9(a)). Fig. 9 (c) clearly indicates that the jacketed P3-500 JCASS cable lose its sensitivity to shear displacement due to slippage between the PE jacket and the outer conductor. This slippage is unfavorable towards the shear deformation transfer to the coaxial cable. This implies that cables with a smooth solid outer conductor should be used without the jacket, while bearing the risk of corrosion to the outer conductor. Compared to the glue bonding between the jacket of P3-500 JCASS and the smooth solid outer conductor, the braided wires of the RG-8 outer conductor grabs the cable jacket tightly due to higher friction resistance, leading to a higher resistance against jacket slippage.

Considering the peak amplitude of reflection pulse, the relationship between peak reflection coefficient (ρ_{peak}) and shear displacement (δ) is shown in Fig. 11. Although P3-500 cables may have a higher signal-to-noise ratio and a stable step pulse with flat background waveform due to lower cable resistance, the reflection amplitude of RG-8 cables can be easily determined by subtracting the measured waveform from an initial waveform prior to shearing. The detectable shear displacement δ_D is defined as the displacement threshold that induces a significant reflection amplitude (ρ_{peak}) greater than 0.002. As shown in Fig. 11, the reflection due to shear displacement can be detected earlier in the RG-8 cable (δ_D = 21 mm) than the bare P3-500 cable (δ_D = 41 mm). RG-8 cable also has a higher overall reflection increase per unit increase of shear displacement in the tested range. This result supports the idea that high-quality braided cables such as RG-8 should be used in soil slopes for early detection of shear displacement. Braided cables do not have slippage problem and are more favorable in terms of corrosion protection, over bare cables with solid outer conductors. It seems that there are no critical reason why braided cables like RG-8 should not be used in rock slopes as well. Due to the slippage problem and its poor sensitivity, P3-500 JCASS (with PE jacket) was not included in subsequent physical model tests.

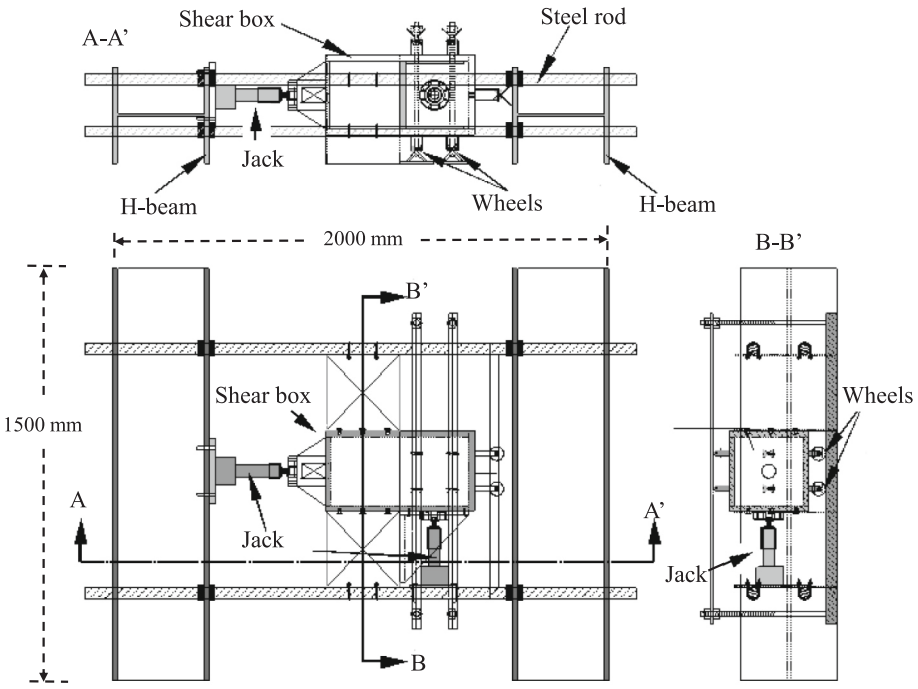

Fig. 5. Detailed design of the large-scale direct shear box.

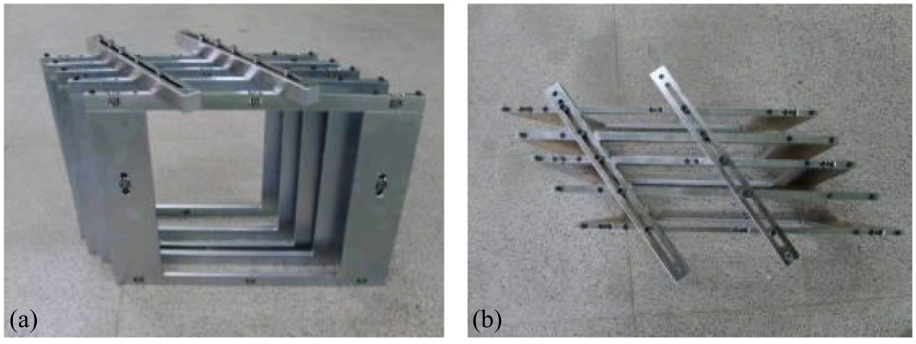

Fig. 6. (a) Side view and (b) top view of the sliding sheets to simulate the shear bandwidth.

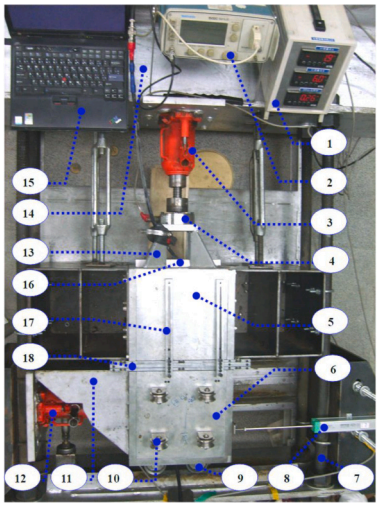

1) Load cell indicators
2) TDR (Tektronix 1502C)
3) Confining jack
4) Confining load cell
5) Top shear box
6) Bottom shear box
7) Steel rods
8) LVDT
9) Shear wheels
10) Vertical wheels
11) Backfill leakage sealer
12) Shearing jack
13) Confining rods
14) H-beam
15) DAQ (laptop computer)
16) Cable-end fixing plate
17) Slide rail
18) Shear bandwidth sliding sheets

Fig. 7. Top-view photo of the large direct shear box and nomenclatures of associated components.

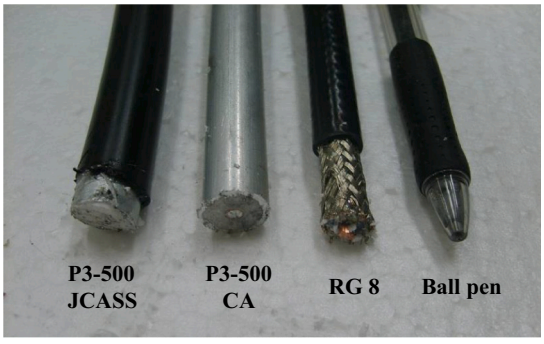

Fig. 8. Three types of coaxial cables used in the direct shear test (enclosed ball pen as the reference scale).

4.2. *Effect of grout layer*

To extend the applicability of TDR in soil slopes, most literatures suggested the installation setup to have a cable-grout composite

Table 1
Specifications of cables.

Cable	CommScope P3-500 JCASS	CommScope P3-500 CA	Belden RG-8
Diameter over center conductor (mm)	2.769	2.769	2.743
Diameter over dielectric (mm)	11.481	11.481	7.239
Diameter over outer conductor (mm)	12.7	12.7	–
Diameter over jacket (mm)	14.478	–	10.29

Table 2
Physical properties of the backfill materials.

Material type	Ottawa sand	Fine gravel
Dry unit weight (kN/m^3)	15.5	16.3
Internal friction angle (degree)	30.7	42.7
D_{60} (mm)	0.39	6.63
D_{30} (mm)	0.31	5.00
D_{10} (mm)	0.26	2.45

compliant to soil stiffness (Pierce, 1998; Cole, 1999; Dowding et al., 2001). Albeit this is the ideal situation, there are limited coaxial cable types, and there may also be variabilities in the in-situ ground characteristics and the grout strength control. In the physical model, we can examine the effect of grout compatibility on the two mainly used coaxial cable types. Coaxial cables were embedded in the large direct shear box without the grout column, representing a perfect compliance of borehole backfills to the surrounding soils. This condition is practically impossible to achieve in the field, but can be simulated in the physical model for ideal comparison with a typical field installation response. Fig. 12(a) and (b) show the measured waveforms of the direct shear test for RG-8 and P3-500 cable directly buried in Ottawa sand, without any grout. Their TDR responses can be compared with Fig. 9(a) and (b) to understand the effect of grout compliance. For soft cable in weak grounds, TDR's response to shear displacement may be enhanced by reducing the grout stiffness to match the surrounding soils. Without the grout, the reflected waveforms of RG-8 cable in sand turn into single bell shape, indicating that the shear deformation is more localized on the shear plane, instead of two particular kinks along the two tension cracks. On the other hand, when the stiff P3-500 cable is used in weak ground, grout compliance to the ground does not increase the TDR's sensitivity to shear displacement.

The quantitative relationship between the reflection amplitude and the shear displacement is shown in Fig. 13. Considering that the grout stiffness used is much higher than the loose sand, the reduction of TDR response for RG-8 in loose sand is not very significant. As for P3-500 cable, which is much stiffer than the loose sand, the grout layer actually helps the loose soil to shear the cable and facilitates the development of TDR response. Grout has low tensile strength. Once the tension cracks on both sides of the shear plane have developed, the stiff-armored grout helps to mobilize the deformation of the stiff P3-500 cable along the cracks, resulting in earlier detection and larger TDR reflection. Based on these observations, a standard formula of grouting (i.e., possessing significant stiffness to shear the embedded cable) for various cable types and ground conditions can be deduced to simplify the installation process of TDR monitoring cables.

4.3. Effect of cable-grout-ground interaction

For a given cable-grout composite installed in the ground, the TDR response depends on the composite and ground interaction. This section examines the cable-grout-ground interaction in two ground conditions (sand and gravel) using two cable-grout composites, which are RG-8 and P3-500, both in 1:1 W/C cement grout. The strength and stiffness of coaxial cables, 1:1 W/C cement grout, and different cable-grout-ground composites are listed in Table 3, confirming that the stiffness is significantly higher in gravel than that in sand. Although the stiffness and strength of coaxial cables are even higher than the grout in terms of material properties, they are slender element and subjected to both bending and elongation during the composite shearing. Fig. 12 (c) and (d) reveal different TDR responses of the two cable types in gravel, in comparison to Fig. 9(a) and (b) with similar setup but embedded in loose sand. Referring to Fig. 10, the distance between the two maximum moments is reduced in gravel due to its higher stiffness. Hence, the stiffer gravel causes more localized shear deformations in the cable, and results in reflection waveforms more like a single bell shape on the dominant side of the cracks. On the contrary, the two moment-induced tension cracks are more separated and lead to double reflection spikes in soft ground. These observations provide more insights on the actual behavior of the cable-grout-ground composite in TDR landslide monitoring, which were not previously revealed by experiments using only the cable-grout composites.

The quantitative comparison of TDR responses (in terms of reflection amplitude in different composites is shown in Fig. 14. Fig. 14 provides benchmarks of TDR responses in different materials. The first two TDR responses in Fig. 14 are the cable-grout composites without surrounding

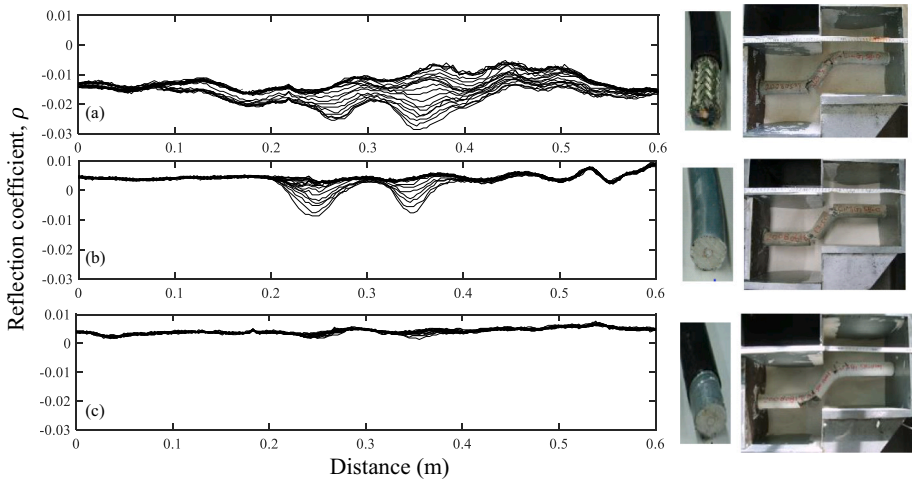

Fig. 9. The reflected waveforms and corresponding photos of the tested specimens (grouted cables) in Ottawa sand (W/C = 1, σ_v=285 kPa), with embedded (a) RG-8 (b) P3-500 CA and (c) P3-500 JCASS with the jacket.

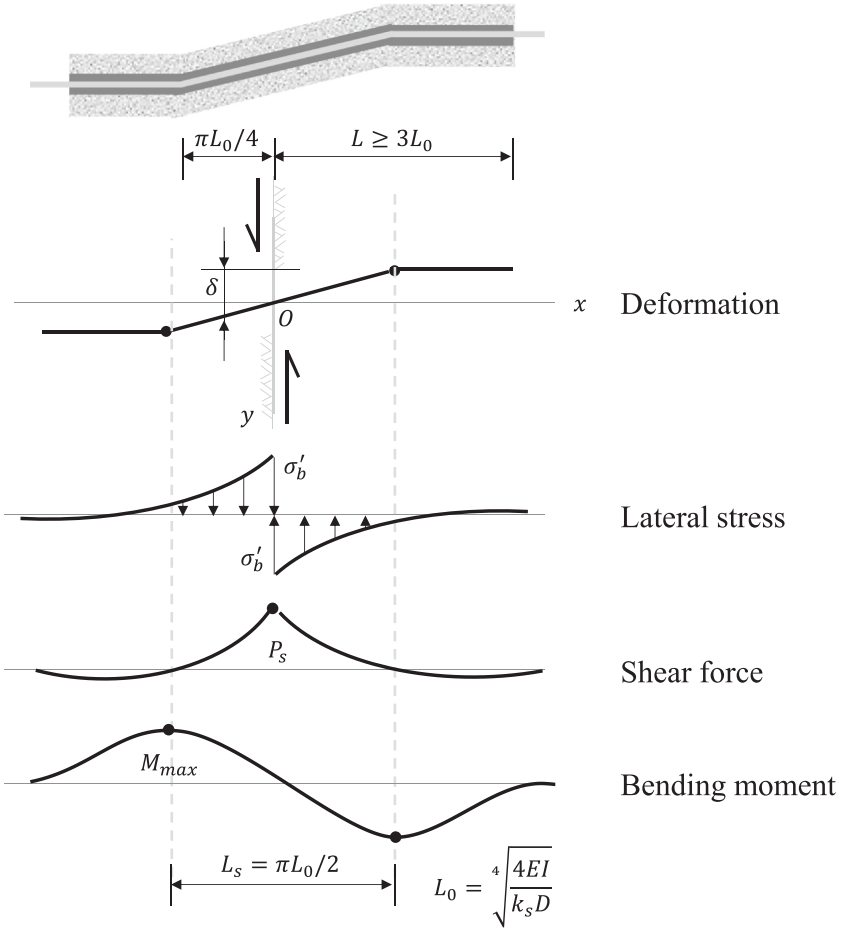

Fig. 10. The displacement and stressed condition of the cable-grout composite (modified from Schlosser, 1982).

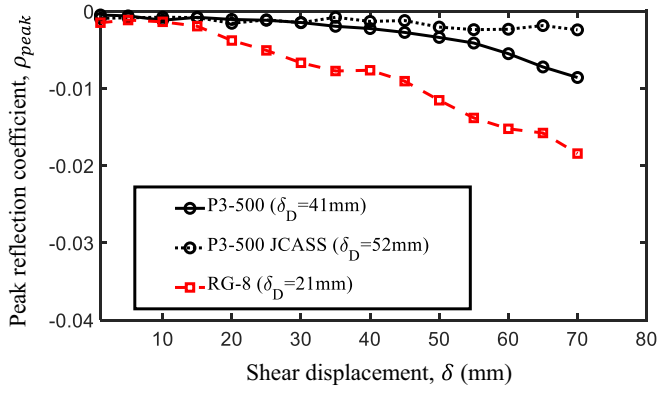

Fig. 11. The relation curve between TDR ρ_{peak} and δ for different types of cables (W/C = 1, Ottawa sand and σ_v = 285 kPa).

soils, which were modified from Lin et al. (2009). The TDR response of cable-grout composite would represent the likely response for any rocks stiffer than 1:1 W/C cement grout. The responses in gravel and sand would represent the likely behavior in stiff soils and soft soils, respectively. The stiff P3-500 cable-grout-gravel composite exhibits a distinct behavior from others. As the shear displacement exceeds the threshold and mobilizes tension cracks, the stiffer gravel can deform the P3-500 cable-grout much more than sand, resulting in a sharper turn in the ρ_{peak}-δ curve, which eventually approaches a similar slope as the cable-grout composite. This can also be observed from the reflection coefficient plot of this setup in Fig. 12(d), where the reflected waveforms beyond the threshold displacement become a single bell shape, similar to that in shearing the cable-grout composite without surrounding soils from Lin et al. (2009).

A closer inspection of Fig. 14 reveals that the displacement threshold δ_D increases as ground stiffness decreases. The differences in displacement threshold and ρ_{peak}-δ slope increase the difficulty in direct deduction/quantification of the absolute shear displacement in the ground from TDR response. The soft RG-8 cable has a smaller displacement threshold and simpler behavior with the ρ_{peak}-δ slope more or less proportional to the ground stiffness. Nevertheless, unique quantification of the shear displacement directly from any TDR response is not possible due to different cable-grout-ground interactions. In this regard, Fig. 14 should only be used as a rough benchmark, whereas the interpretation of TDR response should focus more on the rate of change in reflection amplitude, as also suggested by Chung and Lin (2019) from field application point of view.

4.4. *Effect of shear bandwidth*

In addition to the cable-grout-ground interaction, the width of the localized shear band may affect the TDR response. The influencing mechanism of the shear bandwidth towards the cable-grout composite was investigated using a combination of RG-8 cable, 1:1 W/C cement grout, Ottawa sand, and the aid of the sliding sheets as illustrated in Fig. 4(a) and shown in Fig. 6 and Fig. 7 (marked as component 18). These tests were only conducted in loose sand to model the strain localization in weak materials. The TDR responses and photos of the samples after going through the final stage of shearing are shown in Fig. 15, for shear bandwidth of 0, 3, and 5 cm respectively in subplots

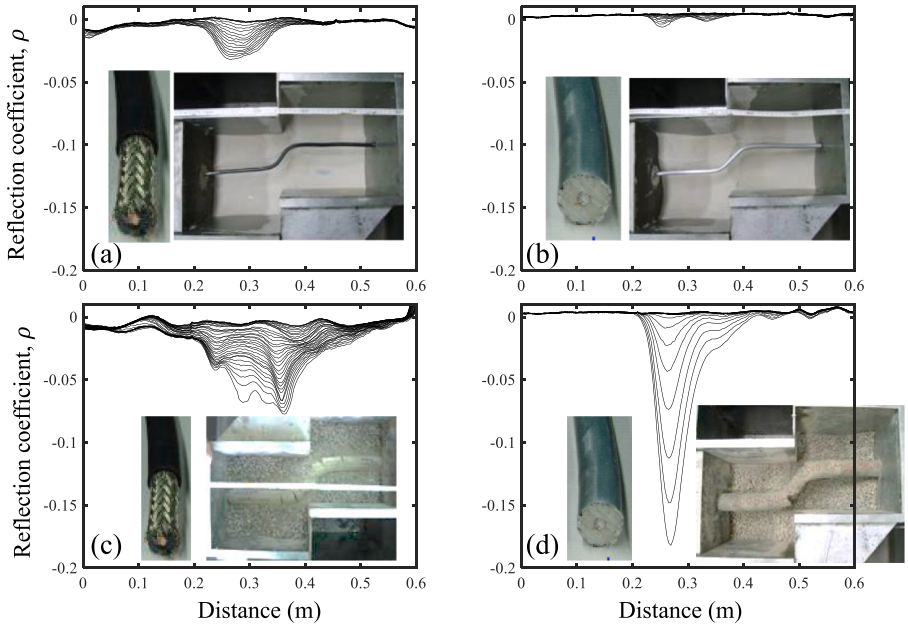

Fig. 12. The reflected waveforms and corresponding photos of the tested specimens for (a) RG-8 without grouting in sand, (b) P3-500 CA without grouting in sand, (c) RG-8 with grouting in gravel, and (d) P3-500 CA with grouting in gravel (W/C = 1, σ_v = 285 kPa).

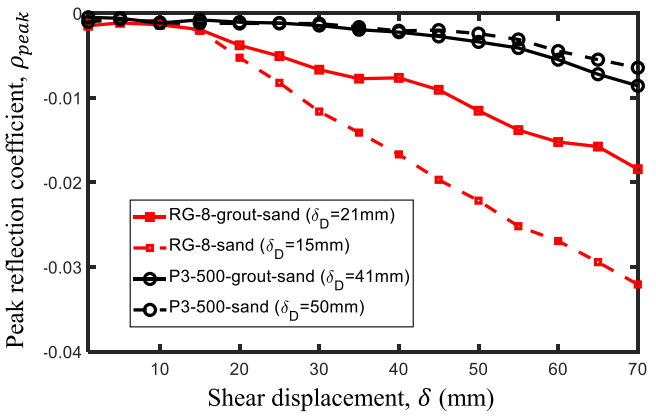

Fig. 13. Effect of grout layer on TDR response (W/C = 1, Ottawa sand, σ_v = 285 kPa).

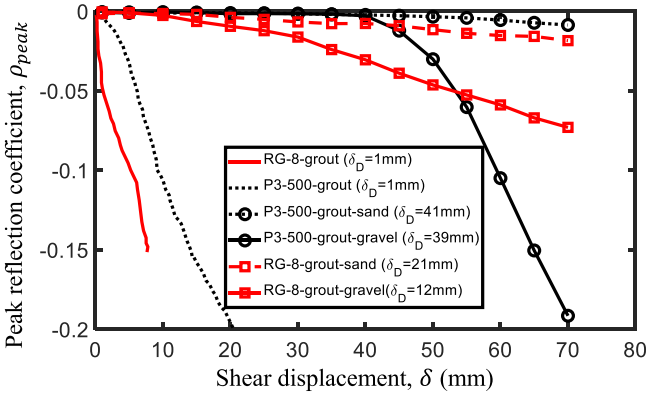

Fig. 14. Effect of cable-grout-ground interaction on ρ_{peak}-δ relation (W/C = 1, σ_v = 285 kPa).

Table 3
Peak shear strength and shear stiffness of cables, grout, and cable-grout-ground composites.

Cable, cement grout, or cable-grout-ground composite	Peak shear strength (kPa)	Shear stiffness (kPa/mm)
P3-500 cable	11,256	1355
RG-8 cable	9118	691
Grout (W/C = 1)	1118	444
Sand + Grout + RG-8 + σ_v (285 kPa)	268	65
Gravel + Grout + RG-8 + σ_v (285 kPa)	432	103

(a), (b), and (c). In all cases, two reflection spikes resulted from the localized cable deformation develop along the two tension cracks. In soft materials like loose sand, the distance between the two tension cracks remains relatively constant regardless of the designated shear bandwidth. As shown in Fig. 16, the quantitative relations between the reflection amplitude and the shear displacement for the three cases with different shear bandwidths are similar. Compared to the observations in different ground conditions, the effect of grout-ground interaction is much more significant than the effect of shear bandwidth. This may be attributed to the phenomenon in which tension cracks would develop at similar locations in brittle grout, regardless of the shear band thickness. Unless the shear bandwidth is much larger than the width between two prominent tension cracks, a similar TDR response is expected for cable-grout composite in weak ground, regardless of the thickness of shear band. For the case of much larger shear bandwidth, it may be treated as two separate shear planes.

5. Data reduction of TDR waveform

The experimental results above show that the braided RG-8 cable is more sensitive for TDR landslide monitoring and is suitable for implementation across a wide range of geo-materials, from weak soils to stiff rocks. Due to the high friction resistance between the braided outer conductor and the PE jacket, the jacketed RG-8 cables would provide better corrosion protection while maintaining high sensitivity to shear deformation. The drawbacks of soft braided cables (e.g. RG-8 cables) are their higher resistance loss and poorer uniformity of characteristic impedance. This can be seen from the raw waveforms in previous figures

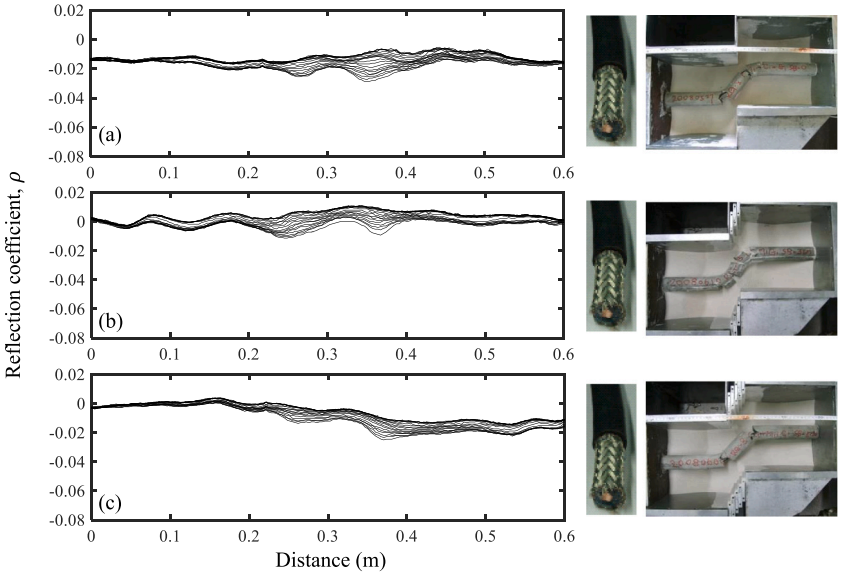

Fig. 15. The reflected waveforms and corresponding photos of the tested specimens of RG-8 with (a) zero bandwidth (b) 3 cm bandwidth, and (c) 5 cm bandwidth in sand (W/C = 1, σ_v = 285 kPa).

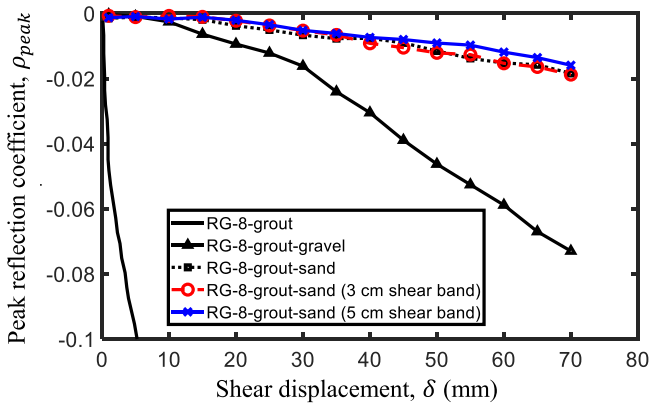

Fig. 16. Effect of shear bandwidth on ρ_{peak}-δ relation for RG-8 cable (W/C = 1, Ottawa sand, σ_v = 285 kPa).

(Figs. 9, 12, and 15), in which the noise levels of RG-8 are apparently higher, and the level regions are not as flat as the P3-500 cable. To mitigate this disadvantage and to automate the early detection of sliding plane development, it is suggested that the time-lapse measurements are processed using differential waveforms, by subtracting the initial (reference) waveform from subsequent ones (Cortez et al., 2009). Fig. 17 illustrates an example of the tested case in Ottawa sand (W/C = 1, σ_v = 285 kPa, and RG-8, as depicted in Fig. 9(a)), where the original waveforms and differential waveforms are plotted in Fig. 17(a) and (b), respectively. The random noise can be easily characterized in the level part of a differential waveform. The standard deviation of the random noise can be calculated and used to identify the occurrence of sliding planes, which is implemented by a three-sigma rule that uses three standard deviations (3σ) as the threshold for detecting reflection events. Signals beyond three standard deviations of the random noise are unlikely, unless there is actually a reflection spike from a developed shear plane. In this example, a reflection spike is detected at a distance near 2.2 m. Although that very reflection variation may also be seen in the raw waveforms from Fig. 17(a), the value contrast is not as noticeable as in the differential waveforms of Fig. 17(b). Furthermore, the noise level in the differential waveforms can also be reduced by signal filtering. Fig. 17(c) shows an example using wavelet filtering on the differential waveforms (Moreau et al., 1996), which is more efficient in noise reduction than the traditional moving average technique. Daubechies 3 (db3) mother wavelet was adopted in the signal filtering of Fig. 17(c) using Matlab®. The filtered results indicate the early detection of a sliding event using the three-sigma rule, in which the shear displacement has only developed for 3 mm. Through integrating all three approaches (i.e., data filtering, differential waveform, and three-sigma rule), early detection of a localized shear plane are shown to have a robust performance and easily automated.

6. Conclusions

TDR is a simple and powerful technique for automated landslide monitoring that is underused. To provide improved guidelines for TDR cable installation and data interpretation, a large direct shear box was devised to realistically model the cable-grout-composite interaction and re-examine several influence factors, including cable type, grout condition, ground condition, and shear bandwidth. Several conclusions can be drawn from the experimental results as follows:

1. Soft cable (e.g., RG-8) and stiff cable (e.g., P3-500 CA) are mechanically suitable for installation in a soil and rock slope, respectively. However, the jacket of any coaxial cable with smooth solid outer conductor should be removed (such as in the P3-500 CA case) to avoid jacket slippage, which would significantly reduce the measurement sensitivity. Considering the dilemma between jacket slippage and chemical corrosion without jacket protection when using a stiff coaxial cable, soft braided coaxial cables (such as RG-8) would be better suited for both soil and rock slope installations.
2. Grout compliance to weak ground can slightly improve TDR response when a soft cable is used. However, a stiff grout does not overprotect the coaxial cable from shear deformation, even in soft grounds. Tension cracks would eventually develop on both sides of the shear plane and mobilize the shear deformation of cable. Hence, a standard grout formula that is significantly stiffer than the installed cable can be used regardless of ground conditions, in order to simplify the construction of TDR installation.
3. The relationship between TDR reflection amplitude and shear displacement is inevitably affected by the cable-grout-ground interaction. If cable-grout composite is standardized, some ρ_{peak}-δ relations can be empirically determined for some reference ground

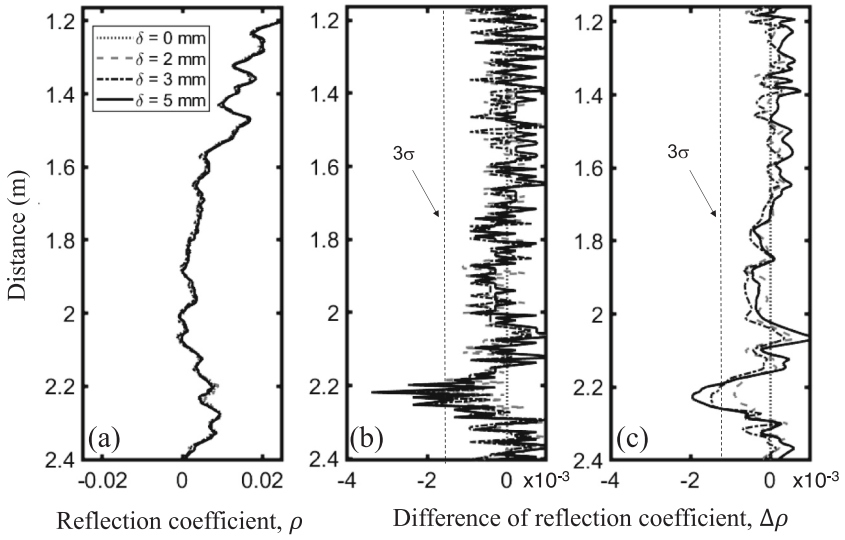

Fig. 17. Data reduction example using RG-8 cable. (a) Raw measured waveforms, (b) differential waveforms (from the initial), and (c) differential waveforms after waveform filtering.

conditions. Since it is not possible to uniquely quantify the absolute shear displacement from a TDR response, the interpretation of the TDR response should focus more on the rate of change in reflection amplitude.

4. The effect of shear bandwidth on ρ_{peak}-δ relation is not significant for the tested range of shear bandwidth (≤5 cm). This may be attributed to the fact that the width between the two prominent tension cracks is larger than the shear bandwidths. In the case of a much larger shear bandwidth, it may be treated as two separate shear planes.
5. To compensate for the higher noise level in the recommended coaxial cable with braided outer conductor, an integrated data reduction approach (including data filtering, differential waveform, and three-sigma rule) is recommended for robust early detection of localized shear plane.

More field implementations will be carried out alongside with other more direct methods (e.g., inclinometer or ShapeArray) to further confirm some of the above findings. It is also suggested to extend the physical model to investigate how to construct the TDR cable together with an inclinometer to combine the merits of both technologies.

Declaration of Competing Interest

The authors declare that they have no known competing financial interests or personal relationships that could have appeared to influence the work reported in this paper.

Acknowledgements

This work was supported by the Ministry of Science and Technology (MOST) of Taiwan under grant number MOST 104-2625-M-009-005.

References

Aimone-Martin, C.T., Oravecz, K.I., Nytra, T.K., 1994. TDR calibration for quantifying rock mass deformation at the WIPP site, Carlsbad, NM. In: Symposium and Workshop on Time Domain Reflectometry. Northwestern University, U.S. Department of Interior, pp. 19–94. Special Publication.

Allasia, P., Godone, D., Giorden, D., Guenzi, D., Lollino, G., 2020. Advances on measuring deep-seated ground deformations using robotized inclinometer system. Sensors 20 (13), 3769.

Barendse, M., Machan, G., 2009. In-place microelectromechanical system inclinometer strings – evaluation of an evolving technology. In: Transportation Research Board 88th Annual Meeting. Washington, DC, pp. 11–15. January.

Belden, 2018. Detailed Specifications & Technical Data of 8214 Coax - RG-8 Type. Belden, Inc.

Blackburn, J.T., Dowding, C.H., 2004. Finite-Element analysis of time domain reflectometry cable-grout-soil interaction. J. Geotech. Geoenviron. Eng. 130 (3), 231–239.

Chung, C.-C., Lin, C.-P., 2011. High concentration suspended sediment measurements using Time Domain Reflectometry. J. Hydrol. 401, 134–144.

Chung, C.-C., Lin, C.-P., 2019. A Comprehensive framework of TDR landslide monitoring and early warning substantiated by field examples. Eng. Geol. 262, 105330 https://doi.org/10.1016/j.enggeo.2019.

Cole, R.G., 1999. Compliant TDR Sensor Cable Grout Composites to Measure Localized Soil Deformation. MS thesis. Dept. of Civil and Environmental Engineering, Northwestern Univ, Evanston, Ill.

Cortez, E.R., Hanek, G.L., Truebe, M.A., Kestler, M.A., 2009. Simplified user's Guide to Time-Domain Reflectometry Monitoring of Slope Stability. National Technology and Development Program. U.S. Department of Agriculture.

Di Maio, C., Vassallo, R., Vallario, M., Pascale, S., Sdao, F., 2010. Structure and kinematics of a landslide in a complex clayey formation of the Italian Southern Apennines. Eng. Geol. 116 (3–4), 311–322.

Dowding, C.H., Huang, F.C., 1994. Early detection of rock movement with time domain reflectometry. J. Geotech. Eng. 120 (8), 1413–1427.

Dowding, C.H., Pierce, C.E., 1994. Measurement of localized failure planes in soil with time domain reflectometry. In: Proc., Symp. on Time Domain Reflectometry in Environmental, Infrastructure, and Mining Applications. U.S. Bureau of Mines, pp. 569–578. Special Publication SP 19-94 NTIS PB95-105789.

Dowding, C.H., Su, M.-B., O'Connor, K.M., 1988. Principles of time domain reflectometry applied to measurement of rock mass deformation. Int. J. Rock Mech. Min. Sci. Geomech. Abstr. 25, 287–297.

Dowding, C.H., Su, M.-B., O'Connor, K.M., 1989. Measurement of rock mass deformation with grouted coaxial antenna cables. Rock Mech. Rock. Eng. 22, 1–23.

Dowding, C.H., Cole, R.G., Pierce, C.E., 2001. Detection of shearing in soft soils with compliantly grouted TDR cable. In: Proc. TDR 2001. Infrastructure Technology Institute, Evanston, Illinois, pp. 5–7. September.

Dowding, C.H., Summers, J.A., Taflove, A., Kath, W.L., 2002. Electromagnetic wave propagation model for differentiation of geotechnical disturbances along buried cables. Geotech. Test. J. 25 (4), 449–458.

Festl, J., 2008. Eignungsprüfung von zement-bentonit suspensionen als injektionsgut bei TDR deformations messungen. Master thesis. Supervised by Kurosch Thuro and John Singer. Technical University Munich, Chair of Engineering Geology, Munich.

Intrieri, E., Gigli, G., Mugnai, F., Fanti, R., Casagli, N., 2012. Design and implementation of a landslide early warning system. Eng. Geol. 147–148, 124–136.

Juran, I., Schlosser, F., 1986. Soil nailing in excavation and slope stabilization. Chapter of NCHRP report. In: Mitchell, J.K., Villet, W.B. (Eds.), No. 290, on Reinforcement of Earth slopes and Embankments. Bulletin of the National Research Council, Transportation Research Board, pp. 258–313.

Kim, M.H., 1989. Quantification of Rock Mass Movement with Grouted Coaxial Cables. MS thesis. Supervised by Dowding, Charles H. Dept. of Civil and Environmental Engineering, Northwestern Univ, Evanston, Ill.

Lin, C.-P., Tang, S.-H., 2006. Comprehensive wave propagation model to improve TDR interpretations for geotechnical applications. Geotech. Test. J. 30 (2), 90–97.

Lin, C.-P., Tang, S.-H., Lin, W.-C., Chung, C.-C., 2009. Quantification of cable deformation with TDR: implications to landslide monitoring. J. Geotech. Geoenviron. Eng. 135 (1), 143–152.

Lin, C.-P., Tang, S.-H., Lin, C.-H., Chung, C.-C., 2015. An improved modeling of TDR signal propagation for measuring complex dielectric permittivity. J. Earth Sci. 26 (6), 827–834.

Moreau, F., Gibert, D., Saracco, G., 1996. Filtering non-stationary geophysical data with orthogonal wavelets. Geophys. Res. Lett. 23 (4), 407–410.
O'Connor, K.M., 1991. Development of a System for Highwall Monitoring Using Time Domain Reflectometry. U.S. Bureau of Mines Summary Rep.
O'Connor, K.M., Peterson, D.E., Lord, E.R., 1995. Development of a highwall monitoring system using time domain reflectometry. In: Proc., 35th U.S. Symp. Rock Mech. Lake Tahoe, Nevada, pp. 5–7. June.
Pasuto, A., Silvano, S., Berlasso, G., 2000. Application of time domain reflectometry (TDR) technique in monitoring the Pramollo Pass Landslide (Province of Udine, Italy). In: Bromhead, E., Dixon, N., Ibsen, M.-L. (Eds.), Landslides in Research, Theory and Practice, Eighth International Symposium on Landslides. T. Telford, London, pp. 26–30. June.
Pierce, C.E., 1998. Time Domain Reflectometry Measurements of Localized Soil Deformation. Ph.D. Dissertation. Supervised by Dowding, Charles H. Dept. of Civil and Environmental Engineering, Northwestern Univ, Evanston, Ill.
Pierce, C.E., Bilaine, C., Huang, F.C., Dowding, C.H., 1994. Effects of multiple crimps and cable length on reflection signatures from long cables. In: Proc., Symp. on Time Domain Reflectometry in Environmental, Infrastructure, and Mining Applications. Evanston, Illinois, pp. 5–7. September.
Reese, L.C., 1983. Handbook on Design of Piles and Drilled Shafts under Lateral Load. U. S. Department of Transportation, Federal Highway Administration, Washington, DC.
Schlosser, F., 1982. Behaviour and design of soil nailing. In: Proceedings of Symposium on Recent Developments in Ground Improvements, Bangkok, pp. 399–413. December.
Simeoni, L., Ronchetti, F., Costa, C., Joris, P., Corsini, A., 2020. Redundancy and coherence of multi-method displacement monitoring data as key issues for the analysis of extremely slow landslides (Isarco valley, Eastern Alps, Italy). Eng. Geol. 267, 105504.
Singer, J., 2010. Development of a Continuous Monitoring System for Instable Slopes Using Time Domain Reflectometry (TDR). Ph.D. Dissertation. Supervised by Kurosch Thuro. Technical University Munich, Chair of Engineering Geology, Munich.
Su, M.-B., Chen, I.-H., Liao, C.-H., 2009. Using TDR cables and GPS for landslide monitoring in high mountain area. J. Geotech. Geoenviron. Eng. https://doi.org/10.1061/(ASCE)GT.1943-5606.0000074.
Sun, Y., Zhang, D., Shi, B., Tong, H.J., Wei, G.Q., Wang, X., 2014. Distributed acquisition, characterization and process analysis of multi-field information in slope. Eng. Geol. 182, 49–62.
Tan, X., Wu, J., Huang, J., Wu, M., Zeng, W., 2018. Design of a new TDR probe to measure water content and electrical conductivity in highly saline soils. J. Soils Sediments 18 (3), 1087–1099.
Thuro, K., Singer, J., Festl, J., Wunderlich, T., Wasmeier, P., Reith, C., Heunecke, O., Glabsch, J., Schuhback, S., 2010. New landslide monitoring techniques – developments and experiences of the alpEWAS project. J. App. Geodesy 4, 69–90.
Topp, G.C., Ferre, P.A., 2000. Measuring Water Content in Soil Using TDR: A State-of-the-Art in 1998 (IAEA-TECDOC–1137). International Atomic Energy Agency (IAEA).
Willenberg, H., Evans, K.F., Eberhardt, E., Spillmann, T., Loew, S., 2008a. Internalstructure and deformation of an unstable crystalline rock mass above Randa (Switzerland): part II—three-dimensional deformation patterns. Eng. Geol. 101 (1–2), 15–32.
Willenberg, H., Loew, S., Eberhardt, E., Evans, K.F., Spillmann, T., Heincke, B., Maurer, H., Green, A.G., 2008b. Internal structure and deformation of an unstable crystalline rock mass above Randa (Switzerland): part Internal structure from integrated geological and geophysical investigations. Eng. Geol. 101 (1–2), 1–14.
Wolter, A., Roques, C., Gröblea, J., Ivy-Ochs, S., Christl, M., Loew, S., 2020. Integrated multi-temporal analysis of the displacement behaviour and morphology of a deep-seated compound landslide (Cerentino, Switzerland). Eng. Geol. 270, 105577.